Vacuum 167 (2019) 77–89

Contents lists available at ScienceDirect

Vacuum

journal homepage: www.elsevier.com/locate/vacuum

Insights on interfacial IMCs growth and mechanical strength of asymmetrical Cu/SAC305/Cu-Co system

Xiaowu Hu[a,*], Chao Li[a], Qinglin Li[b], Guangbin Yi[a]

[a] Mechanical & Electrical Engineering School, Nanchang University, Nanchang, 330031, China
[b] State Key Laboratory of Advanced Processing and Recycling of Nonferrous Metals, Lanzhou University of Technology, Lanzhou, 730050, PR China

ARTICLE INFO

Keywords:
SAC305 lead-free solders
Interfacial reaction
Intermetallic compound
Shear strength
Fracture

ABSTRACT

In this study, a Cu-50Co (50 wt% Co) dual-phase alloy substrate was prepared, which was used to fabricate a sandwich structure of Cu/SAC305/Cu-50Co solder joint. The interfacial microstructure evolution, the growth kinetics and activation energies of intermetallic compounds (IMCs) layer in Cu/SAC305/Cu-50Co solder joints during solid-state aging treatment at different temperatures (120 °C, 150 °C and 180 °C) for various time were investigated. After reflowing at 290 °C for 10 min, an uneven and jagged-shaped (Cu, Co)$_6$Sn$_5$ IMC layer was observed at the SAC305/Cu-50Co interface while scallop-shaped Cu$_6$Sn$_5$ IMC was formed at the SAC305/Cu interface. The thickness of IMCs at both of SAC305/Cu and SAC305/Cu-50Co interfaces increased with increasing aging time and aging temperature during solid-state aging. A (Cu, Co)$_3$Sn phase was formed between the (Cu, Co)$_6$Sn$_5$ IMC and the Cu-50Co substrate, while Cu$_3$Sn IMC layer was observed at the interface between the Cu$_6$Sn$_5$ layer and Cu substrate. After prolonged aging treatment, the higher the aging temperature, the earlier (Cu, Co)$_3$Sn and Cu$_3$Sn IMC appeared. During aging, the difference of the diffusion coefficient of IMCs for SAC305/Cu and SAC305/Cu-50Co interfaces was increasingly reduced, while the activation energies of the total IMC at SAC305/Cu and SAC305/Cu-50Co interfaces were 70.76 and 47.96 kJ/mol, respectively. The shear strength experiments regarding two kinds of as-reflowed solder joints (Cu/SAC305/Cu and Cu/SAC305/Cu-50Co) were carried out. The results showed that the shear strength of the Cu/SAC305/Cu solder joint (49.2 MPa) was slightly lower than that of the Cu/SAC305/Cu-50Co solder joint (61.25 MPa).

1. Introduction

In recent years, lead-free solders have achieved rapid development due to the increasing environmental problems caused by using SnPb solders in electronic packaging [1]. Particularly, Sn3.0Ag0.5Cu (SAC305) solder is the most widely studied and used due to its excellent weldability, reliability and mechanical strength [2–4]. It is well known that the thickness and morphology of the intermetallic compound (IMC) have a great impact on the thermal fatigue life, isothermal shear fatigue life, tensile strength and fracture toughness of solder joints. Especially, the growth and properties of IMC formed at the interface between solders and the substrate surface have influences on the strength and reliability of solder joints [5,6]. Besides, the solid-state aging plays a vital role in influencing the bonding strength of solder joints by changing the IMC thickness and solder microstructure. Therefore, in order to obtain better quality solder joints, it is crucial to better understand and control the reliability of the interfacial reaction between the solder and the substrate [7,8].

In electrical and mechanical interconnection field, solder joint must be able to withstand the high thermal and mechanical loads that occur frequently during operation and use of electronic components at higher temperatures [9,10]. Cu is one of the most widely used materials because it is regarded as the best choice for metal substrates in the electronic packaging industry. Previous study has indicated that metallurgical reactions occur between the liquid solder and the Cu substrate and a Cu-Sn IMC is created at the solder/Cu interface during the soldering process [11]. However, some studies have shown that the interfacial reaction between SAC305 solders and Cu substrate is very intense, which caused the rapid formation and thickening of Cu-Sn IMC at the solder/Cu interface after reflowing and consequently leading a brittle and vulnerable solder joint. Hence, there are serious concerns about the reliability of solder/Cu joints during high temperature service [12–15].

Recently, researchers are looking for more metal materials that can be regarded as the substrate for solder joints to replace the copper substrate. Among them, it is a relatively novel method to obtain an

* Corresponding author.
E-mail address: huxiaowu@ncu.edu.cn (X. Hu).

https://doi.org/10.1016/j.vacuum.2019.05.044
Received 31 January 2019; Received in revised form 29 May 2019; Accepted 30 May 2019
Available online 03 June 2019
0042-207X/ © 2019 Elsevier Ltd. All rights reserved.

alloyed substrate by adding other metal elements to the Cu substrate. For instance, Yu et al. [16] carried out the experiments about the interfacial reaction of Sn and Cu-*x*Zn substrates and pointed out that Cu-*x*Zn materials are a potential UBM for retarding Cu pad consumption in solder joints. Cho et al. [17] have discussed whether the Zn content in Cu-Zn alloy substrate could influence the interfacial reactions. Wang et al. [18] pointed out that Zn alloyed into Cu substrate or Sn solder significantly inhibited the formation of Cu_3Sn and the growth of IMC layer during isothermal aging compared with Sn/Cu joints. Moreover, previous studies have pointed out that Co has caused widespread attention and has been introduced into UBM or surface treatment to improve solder joint performance because of its excellent electromigration resistance, acceptable wettability and better reliability [19]. Wang et al. [20] conducted an experiment of Sn/Co-Cu (less than 10 wt % Cu) interfacial reaction to study the effect of the potential Cu-Co dual-phase alloy substrate on the growth rate of interfacial IMCs layer. Our previous related research found that the interface of the SAC305/Cu-Co joint near the substrate was uneven and jagged [5]. However, a limited number of researches have been undertaken for the effect of adding Co in Cu substrate on the interfacial reaction. Particularly, studies about the interface reaction of the lead-free solder with the Cu-Co dual-phase alloy substrate and the formation of uneven and jagged morphology of IMC are still lacking.

In order to study the theoretical possibility of applying dual-phase alloy substrates to electronic packaging, in this study, we prepared a kind of Cu-50Co (50 wt% Co) dual-phase alloy substrate and innovatively fabricated a sandwich structure of the Cu/SAC305/Cu-50Co solder joint. Moreover, different working temperatures may affect the growth rate of the IMC, the dissolution rate of the substrate, and different reaction products [21]. Therefore, we also investigated the interfacial reactions and IMC growth between the SAC305 solder and the pure Cu substrate and Cu-50Co dual-phase alloy substrate respectively during aging process at three levels of temperatures for various durations. The grain morphology, activation energy and growth kinetics of IMCs formed between SAC305 solder and Cu and Cu-50Co substrate respectively during different aging temperatures were investigated. In addition, we focused on the effect of alloyed substrates on the mechanical properties of Cu/SAC305/Cu-50Co solder joints and carried out shear strength and nanoindentation experiments.

2. Experimental procedures

A sandwich structure of the Cu/SAC305/Cu-50Co solder joint was prepared in this study. Cu-50Co dual-phase alloy substrate was prepared with pure Cu and Co (with a purity than 99.99%) according to their proper weight percentage. Then, we put them together in quartz tubes and placed quartz tubes in a vacuum induction melting furnace. All of the samples were melting at 1500 °C in a vacuum of 4.3×10^{-3} Pa for 20 min, and when melting process was finished, these samples were furnace-cooled to room temperature. After that, these prepared Cu-50Co dual-phase alloy substrates were cut into a piece shape with dimensions of 10 mm × 10 mm × 2 mm. The commercial Sn3.0Ag0.5Cu (SAC305) solder paste (KOKL, Korea) was used in this work. Before soldering, the Cu-50Co dual-phase alloy substrates and the pure Cu plates surface were polished by appropriate sandpapers and 0.1 μm diamond paste, and then rinsed in deionized water. The SAC305solder paste was scribbled evenly on the surface of the pure Cu plate, and then Cu-50Co dual-phase alloy substrate was gently placed on the surface of the pure Cu plate covered with the solder. After that, this assembly samples were placed between two clean steel plates and gently pressed with a cylindrical iron block with a weight of 100g to keep the gap distance between two plates to be about 0.2 mm, as demonstrated in Fig. 1(a). Next, these samples were soldered in reflow oven at 290 °C for 10 min to form the Cu/SAC305/Cu-50Co solder joint with a sandwich structure. In addition, Cu/SAC305/Cu solder joint was also prepared with the same method. All the samples were finished under the same reflowing condition and then cooled in air.

It is well known that the service temperature has a large effect on the interfacial reaction and the quality of the solder joints. After soldering, some of these soldered samples were kept in an as-reflowed condition, while others were subjected to three different isothermal aging treatments (120 °C, 150 °C and 180 °C) for 24, 120, 240 and 360 h in aging oven, respectively. In order to obtain the shear strength of the joints, a shear strength test was carried out between two kinds of solder joints (Cu/SAC305/Cu and Cu/SAC305/Cu-50Co) by using shear testing machine with the shear speed of 2000 μm/s, as schematically presented in Fig. 1(b).

In order to observe the cross section of solder joint, the prepared samples were cut into proper size and mounted in epoxy and then subjected to manually grind down to 2000 grit on a sandpaper. Next, these samples were polished by using 2 and 1 μm diamond paste, and subsequently etched with a solution of 3% HCl + 5% HNO_3 + 92% CH_3OH. The microstructures and compositions of reaction phases and fracture surfaces after the shear test were analyzed by using Scan Electron Microscopy (SEM, FEI QUANTA 200F) and Energy Dispersive Spectrometer (EDS with acceleration voltage of 20 KV). The field-emission transmission electron microscope (FE-TEM) was used to demonstrate the existence of Kirkendall voids and the sample for TEM test was prepared by using a focused ion beam (FIB).

3. Results and discussion

3.1. Interfacial microstructure and EDS analysis of aged Cu/SAC305/Cu-50Co joints

Fig. 2 shows the BEI (back-scattered electron image) micrographs of interfacial IMC layer of Cu/SAC305/Cu-50Co solder joints after soldering at 290 °C for 10 min. It can be seen from Fig. 2(a) that the interface of the sandwich structure of the Cu/SAC305/Cu-50Co solder joint was observed. The pure Cu substrate, SAC305 solder and Cu-50Co dual-phase alloy substrate were in order from top to bottom as presented in Fig. 2(a), which clearly revealed the high contrast difference in morphology of the IMC reaction layers formed between the interface adjacent to Cu substrate and Cu-50Co dual-phase alloy substrate. We could also clearly observe the microstructure of the fabricated Cu-50Co dual-phase alloy substrate in Fig. 2(b). It apparently indicated that the composite substrate had a distinct dual-phase microstructure consisting of Co-rich phase and Cu-rich phase. According to the EDS analysis of these two kinds of different area (spectrums 1 and 2), the Cu-rich phase was bright with composition of 85.60 at. % Cu and 14.40 at. % Co, while the Co-rich phase was dark with composition of 16.42 at. % Cu and 83.58 at. % Co, as shown in Fig. 3(a) and (b), respectively. Previous researches showed [22–25] that the formation of Cu-50Co dual-layer structure was due to the occurrence of liquid phase separation, meanwhile the coexistence of Cu-rich solid solution and Co-rich solid solution phases in Cu-50Co alloys was observed, and the white and dark areas represented Cu-rich and Co-rich phases, respectively. As shown in Fig. 2(b), there was one interfacial reaction layer which was not dense enough on the Cu-50Co side after reflowing. We observed that the microstructure of this IMC adjacent to solder exhibited elongated shape and the IMCs tended to extend to the inside of the solder, while an irregularity shape IMC formed on the Cu-50Co dual-phase alloy substrate side. Additionally, it can be clearly seen that the recessed and raised portions of IMCs were adjacent to the Cu-rich and Co-rich phases, respectively. In order to ascertain the major phase of the compounds, the EDS analysis of IMC was implemented and the composition of the IMC phase was confirmed to be 6.69 at. % Co, 47.54 at. % Cu and 45.77 at. % Sn, as illustrated in Fig. 3(c). The atomic ratio of (Cu + Co) to Sn was (47.54 + 6.69): 45.77, which was determined to be the $(Cu, Co)_6Sn_5$ phase. Similar composition of IMC was reported in previous study by Wang et al. and they indicated that $(Cu, Co)_6Sn_5$ meant Cu_6Sn_5 phase with high Co content [20]. Some studies have reported that the

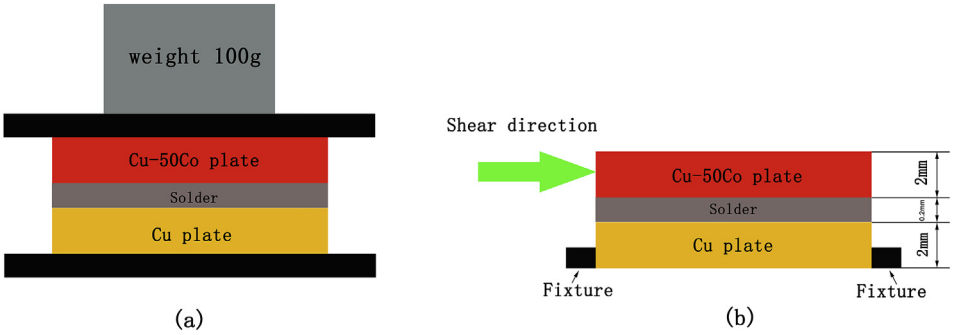

Fig. 1. (a) Installation instruction of Cu/SAC305/Cu-50Co solder joint, (b) sketch of the Cu/SAC305/Cu-50Co solder joint shear sample.

formation of similar structural compounds of (Cu, Ni)$_6$Sn$_5$ phase, and revealed that it was reasonable that the substitution of Ni into Cu$_6$Sn$_5$ without causing lattice distortion or formation of a new phase [26–28]. Furthermore, Dong et al. [29] confirmed that the (Cu, Ni)$_6$Sn$_5$ has the same Cu$_6$Sn$_5$-based crystal structure.

Fig. 2(c) shows the micrograph of interface on the Cu side after reflowing at 290 °C for 10 min. Unlike the interface of SAC305/Cu-50Co, only one uniform reaction layer with scallop-shaped morphology formed at the interface of SAC305/Cu and it was identified as Cu$_6$Sn$_5$ phase according to Fig. 3(d). As shown in Table 1, the average thickness of IMCs of the SAC305/Cu interface was 5.06 μm, while that of the SAC305/Cu-50Co interface was 3.71 μm. This observation indicated that the addition of Co in a pure copper might inhibit the growth of IMC during soldering. Chen et al. [30] mentioned that Ni-Co alloys were regarded as diffusion barriers, and Co was another diffusion barrier layer material of UBM. Hence, in order to systematically investigate the growth behavior and morphology of IMCs in Cu/SAC305/Cu-50Co system during solid-state aging process at different temperatures, thermal aging of the Cu/SAC305/Cu-50Co joints was performed at 120, 150, and 180 °C for aging durations of 24, 120, 240, 360 h, respectively. Fig. 4 shows the cross-sectional micrographs of IMCs for the interface of Cu/SAC305/Cu-50Co solder joints aged at 120 °C for 24, 120, 240, 360 h. On the side of Cu-50Co dual-phase alloy substrate, only a single uneven reaction layer formed after aging at 120 °C for various aging durations, which was regarded as (Cu, Co)$_6$Sn$_5$ phase. Particularly, the IMCs grew gradually towards to the solder, and some coarse compounds could be observed in the middle of bulk solder after aging for 24 h, as shown in Fig. 4(b). These coarse compounds were identified as (Cu, Co)$_6$Sn$_5$ phases composed of 0.84 at. % Co, 51.34 at. % Cu and 47.81 at. % Sn, as confirmed by the EDS analysis of spectrum 5 presented in Fig. 7(a). The Co solubility in the (Cu, Co)$_6$Sn$_5$ phase was only 0.84 at. % based on the Cu$_6$Sn$_5$ structural model. It was implied that the dissolving rate of Co atoms from substrate into solder to form IMCs was much lower than that of Cu atoms during aging, and the reason why the morphology of IMCs was uneven would be further revealed in following analysis.

Similarly, on the side of Cu, the thickness of Cu$_6$Sn$_5$ layer increased progressively, meanwhile a thin dark layer appeared between Cu$_6$Sn$_5$

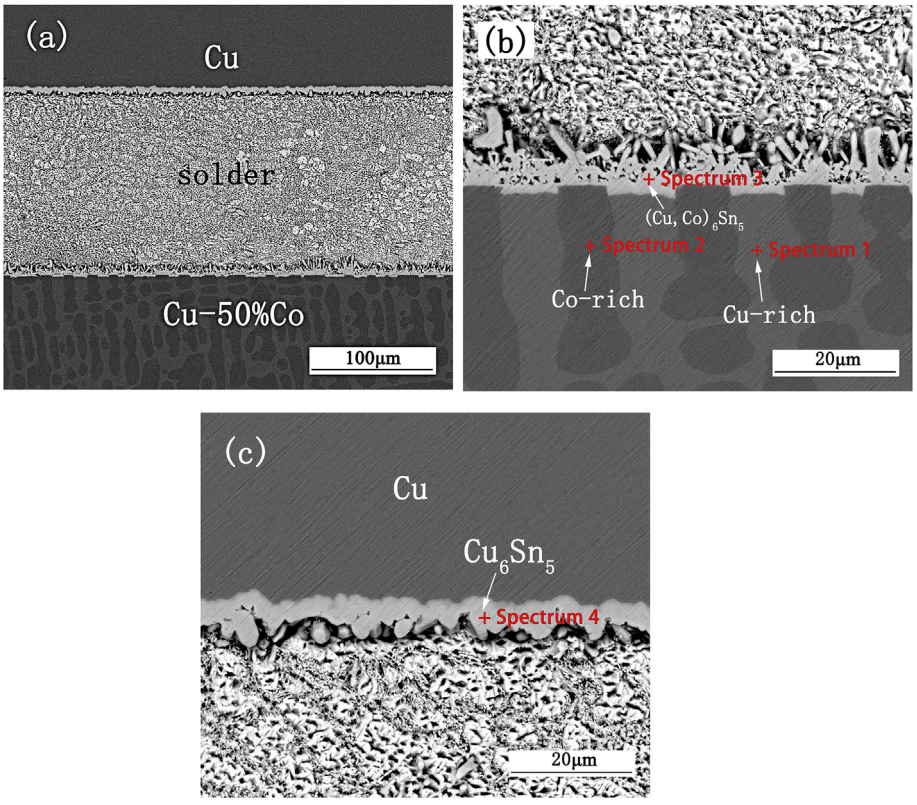

Fig. 2. Cross-sectional microstructure of Cu/SAC305/Cu-50Co solder joints reflowed at 290 °C for 10 min. (a) sandwich structure of the Cu/SAC305/Cu-50Co solder joint. (b) the interface of SAC305/Cu. (c) the interface of SAC305/Cu-50Co.

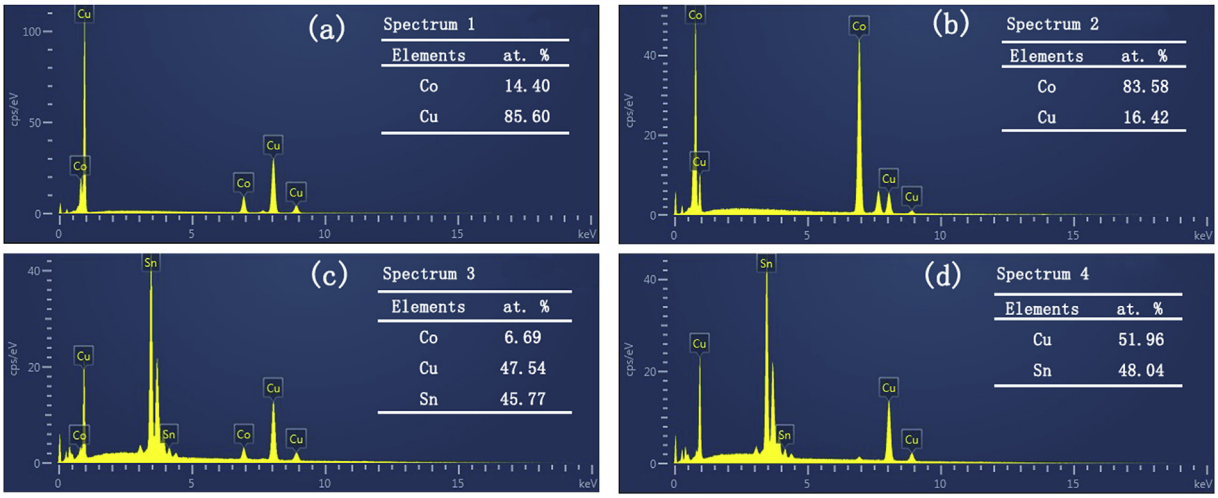

Fig. 3. EDS analysis results for Fig. 2, (a) spectrum 1, (b) spectrum 2, (c) spectrum 3, (d) spectrum 4.

Table 1
Results of statistical data for the IMC thickness of Cu/SAC305/Cu-Co joints.

Aging time/(h)	Total IMCs thickness/μm					
	SAC305/Cu IMC			SAC305/Cu-50Co IMC		
	120 °C	150 °C	180 °C	120 °C	150 °C	180 °C
0	5.060			3.715		
24	5.138	6.041	8.816	4.387	5.273	6.914
120	5.207	7.367	10.351	5.166	6.058	12.571
240	5.459	8.162	14.217	5.298	7.455	15.937
360	5.855	8.406	17.913	5.590	8.391	16.191

phase and Cu substrate with increasing aging time, as shown in Fig. 4(l). According to the EDS analysis of spectrum 6, the thin dark layer adjacent to Cu substrate was considered to be Cu_3Sn phase which was composed of 72.92 at. % Cu and 27.08 at. % Sn, as illustrated in Fig. 7(b). Unlike the interface on the Cu side after reflowing, it could be seen that the Cu_3Sn phase formed in solid-state aging process, and the higher aging temperature or the longer time aging treatment would promote the formation of Cu_3Sn phase. The formation mechanism of the Cu_3Sn compounds during aging could be clarified by formula (2) [7]:

$$Cu_6Sn_5 + 9\ Cu \rightarrow 5\ Cu_3Sn \quad (1)$$

It can be elucidated that abundant Cu atoms could dissolve into Cu_6Sn_5 phase that formed after reflowing to form Cu_3Sn phase during solid-state aging. In addition, the long-time aging treatment with high temperature could accelerate the diffusion of Cu atoms from substrate into IMC layer to participate in the reaction with initial Cu_6Sn_5 phase, which led to the formation of Cu_3Sn phase and the increase of total IMC thickness in following aging process.

Fig. 5 illustrates the cross-sectional microstructure of Cu/SAC305/Cu-50Co solder joints aging at 150 °C for 24, 120, 240 and 360 h, respectively. During aging process with this intermediate temperature, $(Cu, Co)_6Sn_5$ phase was still the dominant reaction layer between solder and Cu-50Co substrate, and the formation of the $(Cu, Co)_6Sn_5$ phase would contribute to the growth of total IMC. It was noteworthy that a discontinuous dark IMC layer appeared between $(Cu, Co)_6Sn_5$ phase and Cu-rich phase, as marked by red circles in Fig. 5(h) and (k). The EDS results confirmed that this IMC was composed of 18.02 at. % Co, 57.35 at. % Cu and 24.63 at. % Sn, as presented in Fig. 7(c). Therefore, the atomic ratio of (Cu + Co) to Sn was (57.35 + 18.02): 24.63, which was close to the chemical composition of $(Cu, Co)_3Sn$ phase. According to the composition, this reaction layer was actually based on the Cu_3Sn phase with some Co solubility. Previous literatures [31,32] pointed that Co atoms in the $CoSn_3$ layer were partly substituted by Cu and Pd atoms from the solder and substrates to form the $(Co, Cu, Pd)Sn_3$ phase, which agreed well with the our results that the $(Cu, Co)_3Sn$ IMC formed since Cu atoms in Cu_3Sn IMC were partly replaced by Co atoms. Compared with the composition of $(Cu, Co)_6Sn_5$ IMC, it was observed that the concentration of Co and Cu increased while the concentration of Sn decreased in $(Cu, Co)_3Sn$ IMC. Similar to the formation of Cu_3Sn phase, initial $(Cu, Co)_6Sn_5$ grains participated in the reaction with Cu and Co atoms to form the $(Cu, Co)_3Sn$ phase. In addition, during the long-time and high-temperature aging treatment process, Sn atoms were inclined to dissolve quickly into the initial $(Cu, Co)_6Sn_5$ compounds, subsequently these $(Cu, Co)_6Sn_5$ compounds consumed Sn atoms and transformed into $(Cu, Co)_3Sn$ compounds, resulting in the decrease of Sn content in $(Cu, Co)_3Sn$ phase. It was worth mentioning that some Kirkendall voids were detected at the interface between IMC layer and Cu-rich phase, as marked by white circles in Fig. 5(e), (h) and (k). In order to clearly observe the morphology of Kirkendall voids, FIB and TEM test were conducted. Fig. 5(m) show the bright field TEM image of interface between IMC layer and Cu-Co substrate, which was obtained from the samples aged at 150 °C for 120 h. As seen from the TEM image, some Kirkendall voids with 95–330 nm in diameter were clearly observed between IMC layer and Cu-rich phase, as indicated by the arrows. The formation mechanism of Kirkendall voids was that Cu atoms from Cu-rich phase in Cu-50Co dual-phase substrate could diffuse into the solder, resulting in the formation of vacancies. As the aging time increased, these vacancies were merged into voids and appeared at the interface of $(Cu, Co)_3Sn$/Cu-rich. This was consistent with the formation of Kirkendall voids at the Cu/Cu_3Sn interface, which was resulted from the unbalanced inter-diffusion of Cu and Sn atoms. As shown in Fig. 5(f), Cu_3Sn phase was found obviously between the Cu substrate and Cu_6Sn_5 phase after aging at 150 °C for 120 h. Compared with the solder joints aged at 120 °C (360 h), the Cu_3Sn phase appeared more earlier in the interfacial IMC layer of solder joints aged at 150 °C (120 h). This result clarified that high temperature would accelerate the formation of Cu_3Sn phase.

Fig. 6 shows the cross-sectional microstructure of Cu/SAC305/Cu-Co solder joints aging at 180 °C for 24, 120, 240 and 360 h, respectively. During this temperature condition, the $(Cu, Co)_6Sn_5$ compounds gradually grew thick towards to solder, meanwhile intermittent $(Cu, Co)_3Sn$ compounds were observed between $(Cu, Co)_6Sn_5$ phase and Cu-rich phase on the side of Cu-50Co dual-phase alloy substrate, as shown by red circles in Fig. 6(e). With increasing aging time, the interfacial IMC layer with an irregular shape adjacent to the Cu-50Co substrate was distinctly apparent, which was due to the reaction rate of the liquid Sn from solder with the Cu-rich phase was faster than that of the liquid

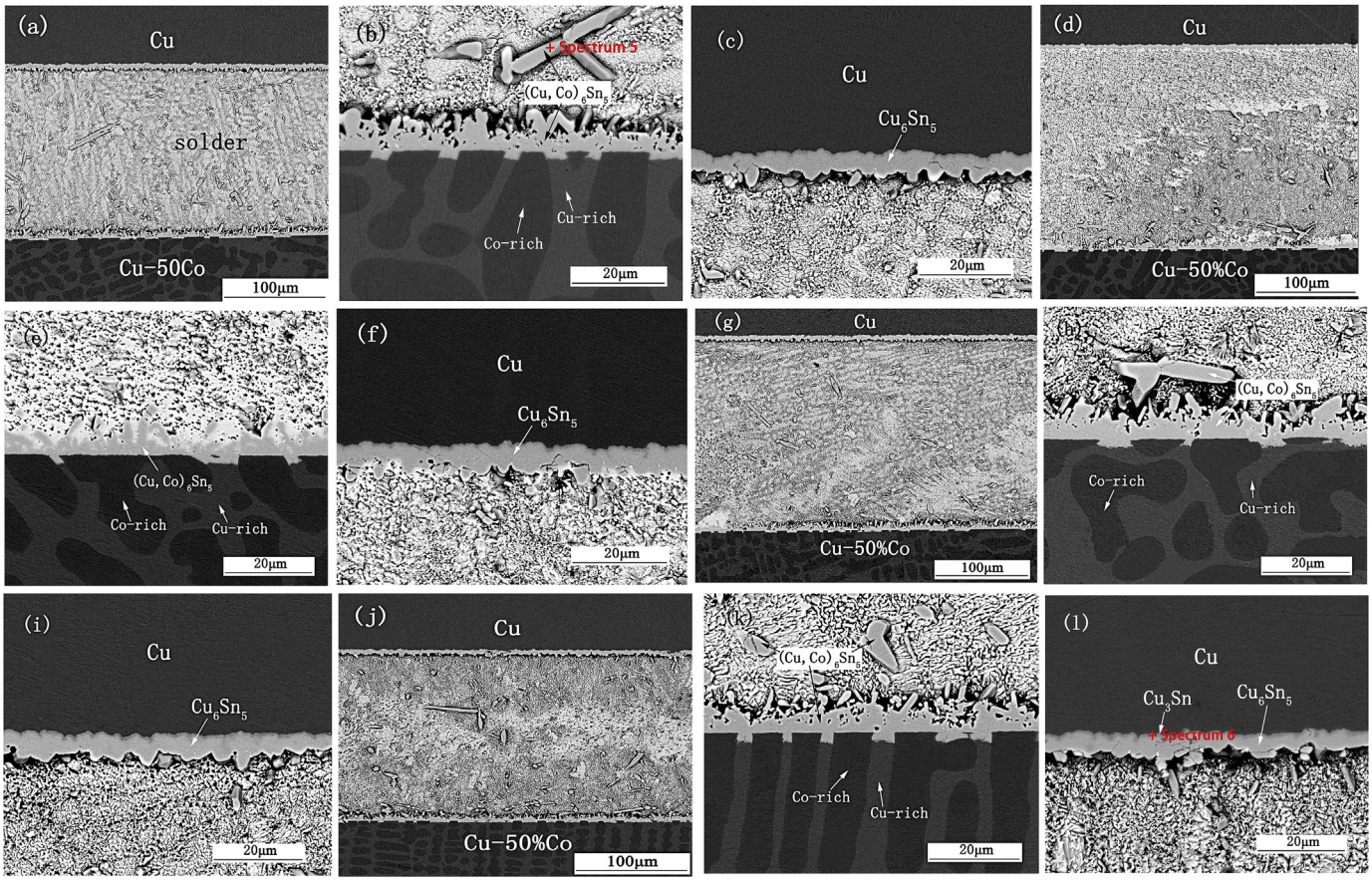

Fig. 4. Cross-sectional microstructure of Cu/SAC305/Cu-50Co solder joints aging at 120 °C for various time, (a)-(c) 24 h; (d)-(f) 120 h; (g)-(i) 240 h; (j)-(l) 360 h.

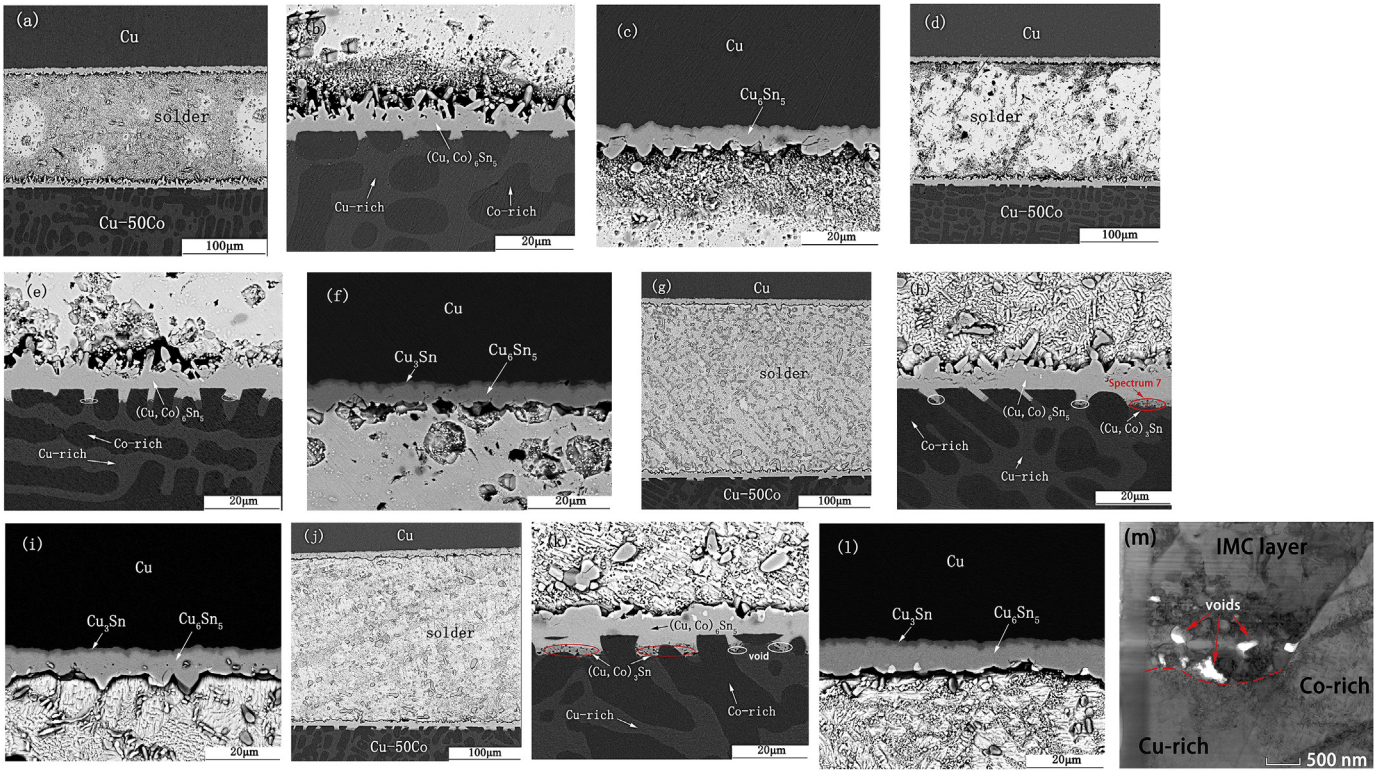

Fig. 5. Cross-sectional microstructure of Cu/SAC305/Cu-50Co solder joints aging at 150 °C for various time, (a)-(c) 24 h; (d)-(f) 120 h; (g)-(i) 240 h; (j)-(l) 360 h; (m) the BF-TEM test for Kirkendall voids.

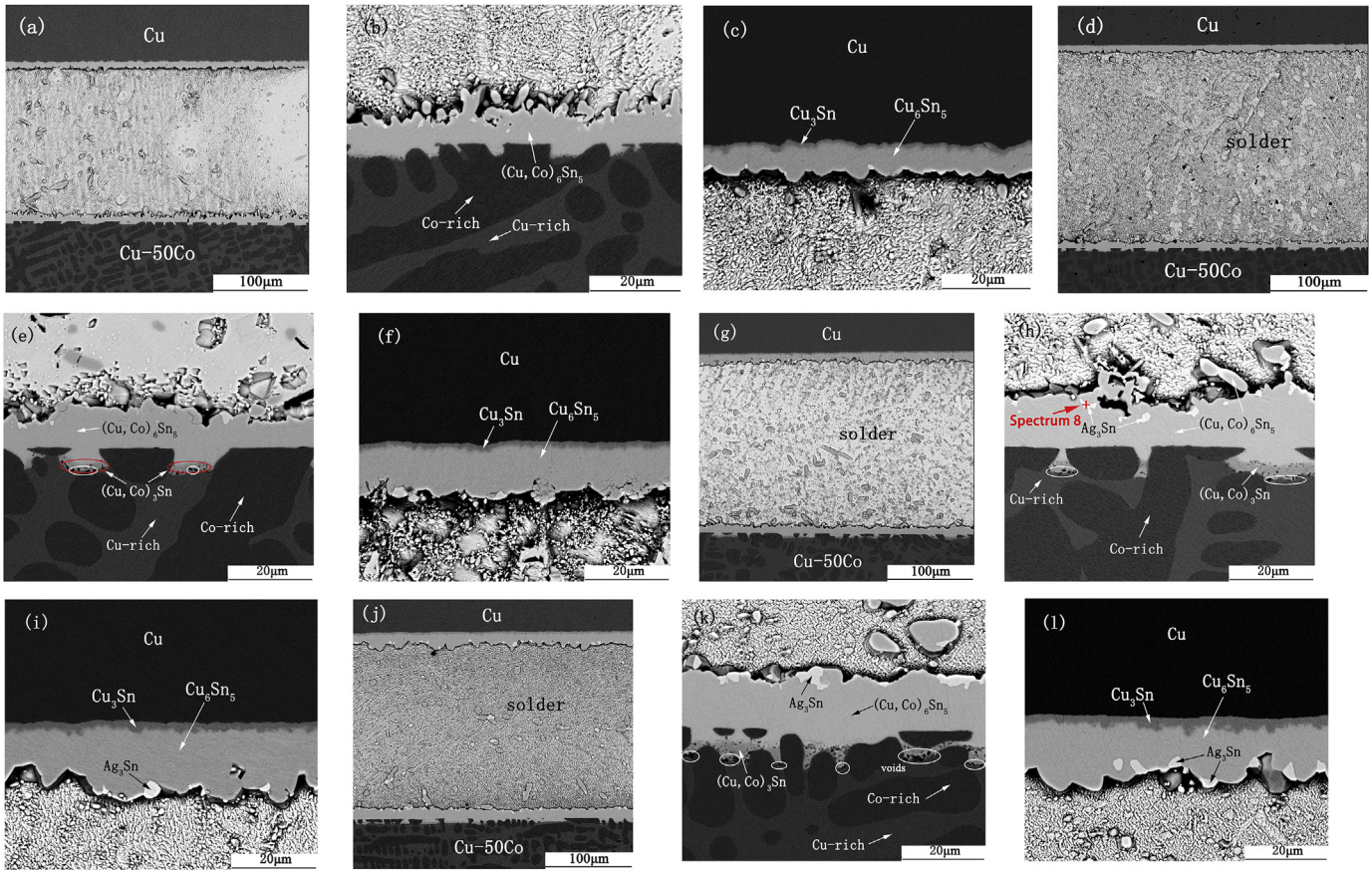

Fig. 6. Cross-sectional microstructure of Cu/SAC305/Cu-50Co solder joints aging at 180 °C for various time, (a)-(c) 24 h; (d)-(f) 120 h; (g)-(i) 240 h; (j)-(l) 360 h.

Sn with Co-rich phase during reflowing. According to literature [33], the solubility of Cu and Co in liquid Sn was about 11 at. % and 0.5 at. % at the temperature of 400 °C, so the reaction rate of Cu-rich phase and Co-rich phase with liquid Sn was distinctly different. Hence, the consumption rate of Cu-rich phase was higher than that of Co-rich phase at the SAC305/Cu-50Co reaction interface on the side of Cu-50Co dual-phase substrate, and the consumption difference of Cu-rich phase and Co-rich phase became more and more obvious as the solid-state aging, ultimately resulting in an irregular and uneven shape interface between IMC reaction layer and Cu-50Co substrate. Moreover, some Kirkendall voids were observed in $(Cu, Co)_3Sn$ phase during aging, which agreed well with the explanation that the higher aging temperature would significantly promote the formation and growth of Kirkendall voids [34]. On the side of pure Cu substrate, the thickness of total IMCs (both Cu_6Sn_5 and Cu_3Sn) visibly increased with increasing aging time during high temperature (180 °C) aging. In addition, the Cu_3Sn phase was observed at the interface between Cu_6Sn_5 phase and Cu substrate after aging at 180 °C only for 24 h, which was very different to the samples that were aging at 120 °C and 150 °C. These results indirectly confirmed that high temperature was conducive to the formation of Cu_3Sn phase. Besides, it should be noted that a small number of white particles were observed in IMC layer at SAC305/Cu-50Co and SAC305/Cu interfaces,

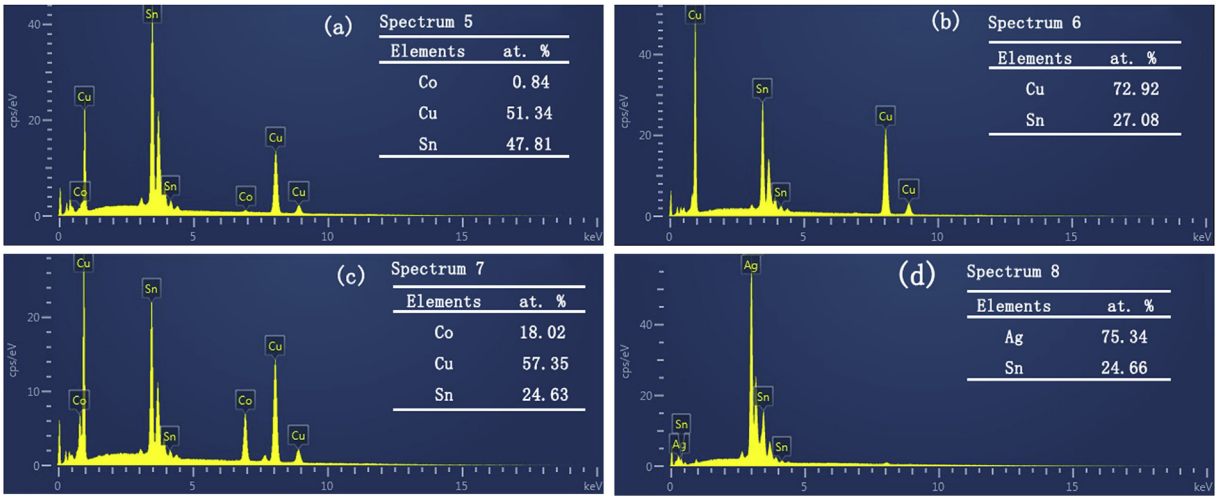

Fig. 7. EDS analysis results for Figs. 4–6, (a) spectrum 5, (b) spectrum 6, (c) spectrum 7 and (d) spectrum 8.

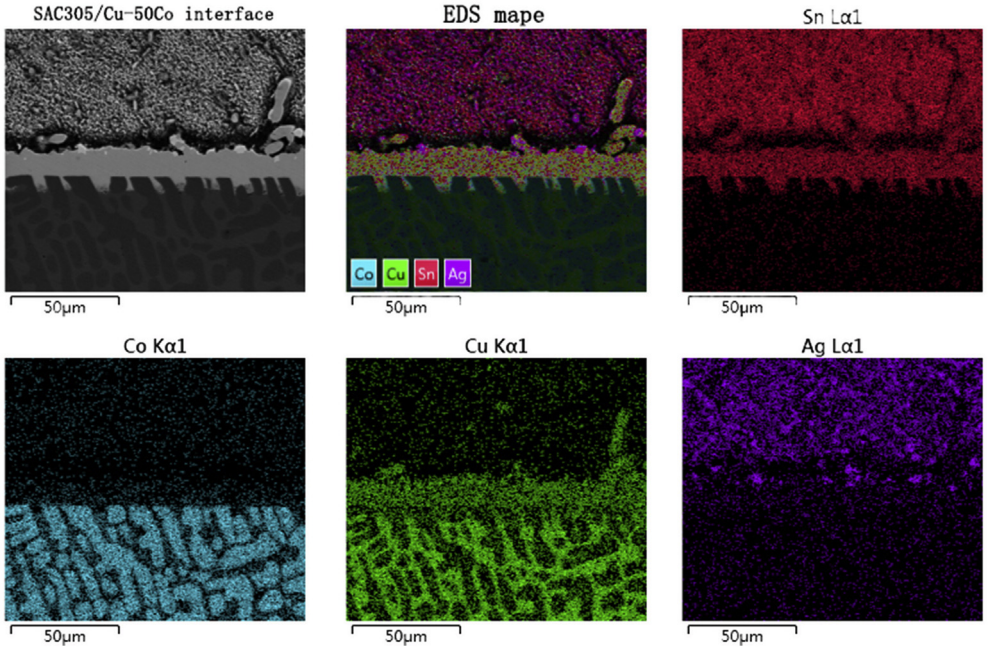

Fig. 8. EDS elements maps of the SAC305/Cu-50Co interface after aging at 180 °C for 360 h.

which was identified as Ag_3Sn phase according to the composition with 75.34 at. % Ag and 24.66 at. % Sn, as shown in Fig. 7(d). With increasing aging time, Ag_3Sn particles became bulkier and increasingly accumulated in IMC layer adjacent to the solder. Li et al. [35] pointed out that Ag_3Sn IMC could exist either as dispersed particles or large branched structures, the latter may have an impact on the interconnect integrity.

Figs. 8 and 9 show the EDS elements maps of the interface in sandwich structure of Cu/SAC305/Cu-50Co solder joint after aging at 180 °C for 360 h. According to EDS elements maps, the unique microtopography structure of Cu-rich and Co-rich phase in Cu-50Co dual-phase alloy substrate was observed evidently, as shown in Fig. 8. Moreover, it could be seen that the morphology of IMC adjacent to the Cu-50Co dual-phase alloy substrate in SAC305/Cu-50Co interface was uneven and presented a jagged shape, which was completely different from the smooth morphology interface of SAC305/Cu in Fig. 9. Cu element with green color was mainly consisted in Cu-rich phase in substrate and widely distributed in IMC layer and solder. Meanwhile, Co element with blue color was principally observed in Co-rich phase, and a small part of them marginally existed in IMC layer and solder. It can be deduced that Cu atoms were more likely to diffuse towards to the solder to take part in the reaction with Sn atoms, compared with Co atoms. In other words, Cu atoms in the Cu-rich phase were consumed more faster than Co atoms in the Co-rich phase, which further accelerated the formation of the IMC with uneven and serrated-shape microtopography.

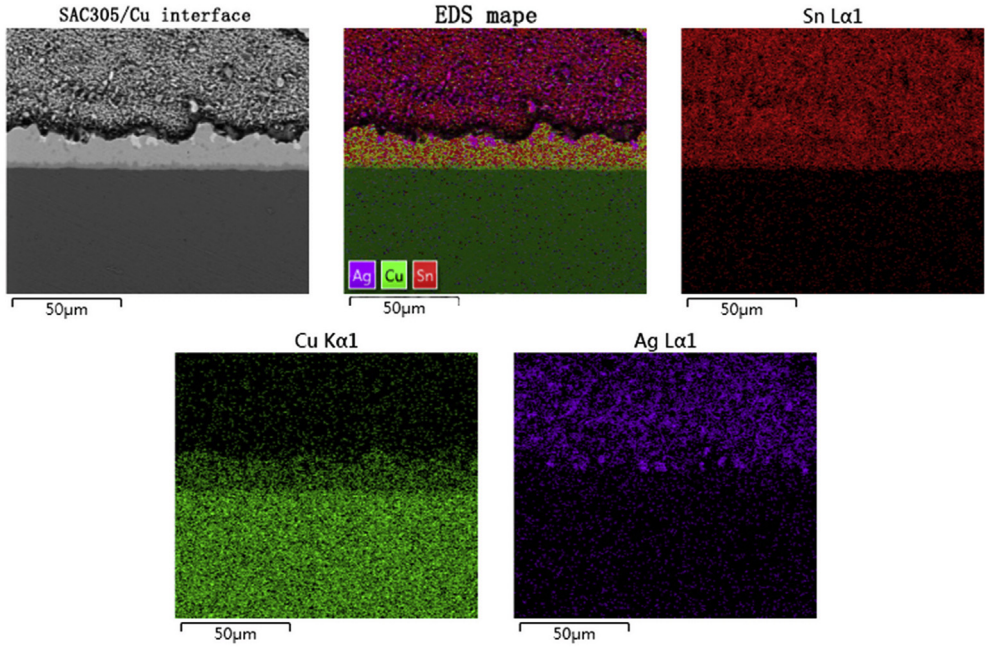

Fig. 9. EDS elements maps of the SAC305/Cu interface after aging at 180 °C for 360 h.

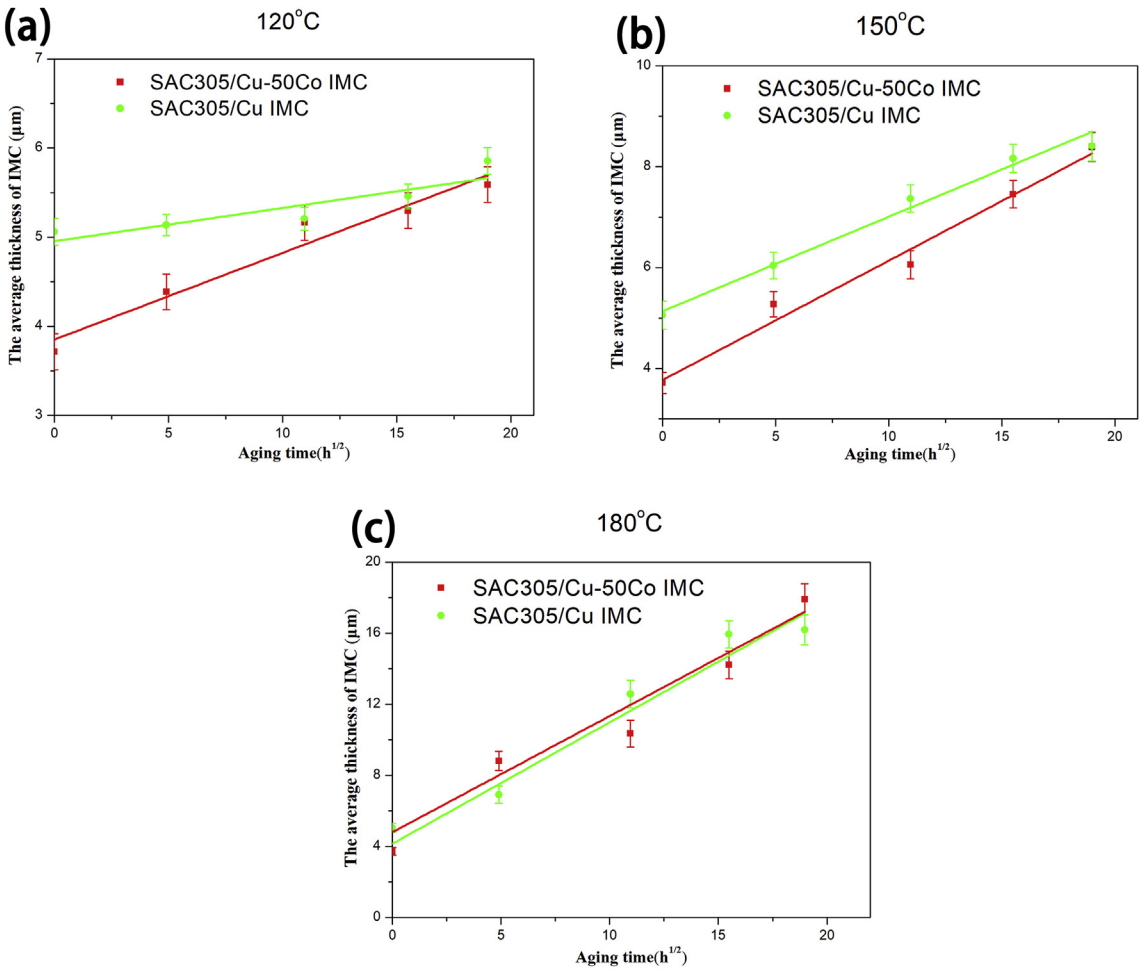

Fig. 10. Thickness of the IMC of SAC305/Cu and SAC305/Cu-50Co interface in Cu/SAC305/Cu-50Co systems with the square root of aging time. (a) aging at 120 °C, (b) aging at 150 °C, (c) aging at 180 °C.

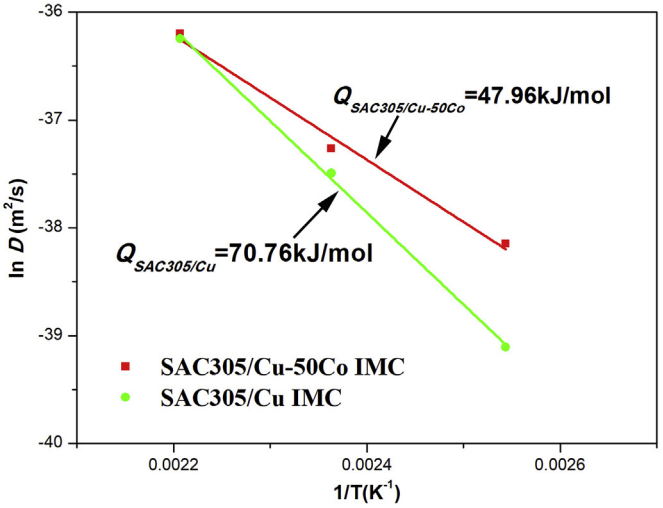

Fig. 11. Arrhenius plots for the IMC growth at the SAC305/Cu-50Co and SAC305/Cu interfaces.

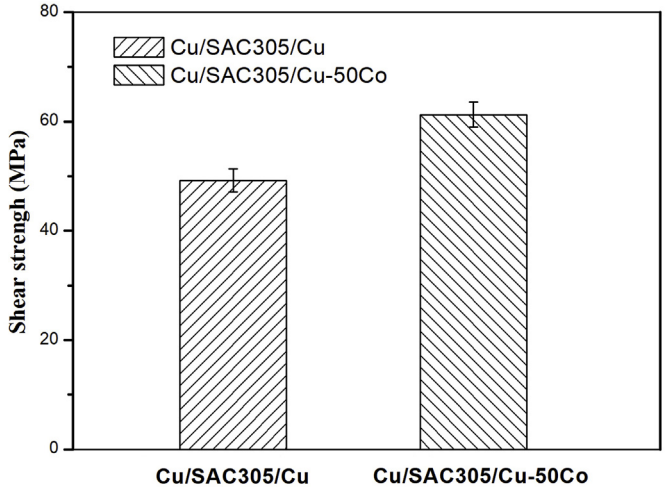

Fig. 12. Shear strengths of Cu/SAC305/Cu and Cu/SAC305/Cu-50Co solder joints after reflowing at 290 °C for 10 min.

3.2. The IMC growth behavior of Cu/SAC305/Cu-50Co joints

The average thicknesses of IMCs of both SAC305/Cu-50Co and SAC305/Cu interfaces in Cu/SAC305/Cu-50Co systems were listed in Table 1. Fig. 10(a)-(c) show the relationship between the square root of aging time and the average thickness of IMC layer of SAC305/Cu and SAC305/Cu-50Co interfaces in Cu/SAC305Cu-50Co joints which were reflowed at 290 °C for 10 min and aged at 120 °C, 150 °C and 180 °C for various time, respectively.

Previous research [36] indicated that the distinction in governing mechanisms of the interfacial IMC growth for Sn-3.5Ag/Cu system,

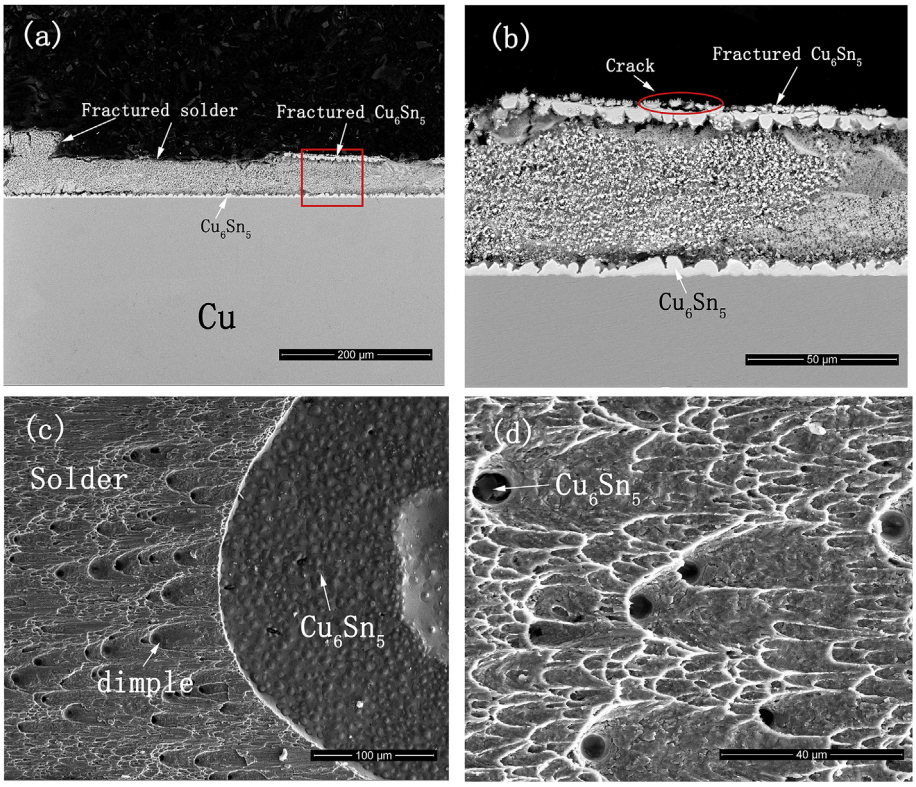

Fig. 13. The SEM photographs of Cu/SAC305/Cu solder joints after reflowing at 290 °C for 10 min subjected to shear fracturing, (a)-(b) the cross-sectional microstructure of SAC305/Cu interface, (c)-(d) the shear fracture top-view morphologies of the samples.

including chemical reaction-controlled growth at initial stage (liquid-solid reaction) and diffusion-controlled growth at final stage of IMC formation (solid-solid diffusion). In current study, the formation of interfacial IMC in Cu/SAC305/Cu-50Co solder joint was controlled by chemical reaction between liquid-state solder and solid-state substrate during soldering, while, in solid-state aging, the growth of IMC was predominantly controlled by atom diffusion mechanism between solid-state solder and substrate. As a result, it is believed that the relationship between the thickness of IMC layers formed during solid-state aging process and the aging duration would be expressed by the following equation [37,38]:

$$x = x_0 + kt^{1/2} \quad (2)$$

where x is the thickness of the IMC layer corresponding various time t at different conditions during aging treatment, x_0 is the initial thickness of the IMC layer after reflowing, k is the diffusion coefficient which plays a crucial role in the growth of the interface IMCs layer. The diffusion coefficient k can be obtained from a linear regression analysis of the line in Fig. 10, where the slope of the line is numerically equal to the diffusion coefficient k. According to fitted results, the values of the diffusion coefficient k of the IMC layers of SAC305/Cu-50Co and SAC305/Cu interface in Cu/SAC305/Cu-50Co solder joints aged at 120 °C were calculated to be about 0.09731 and 0.03734 μm/h$^{1/2}$ (equal to $2.703 \times 10^{-17}$and 1.037×10^{-17} m^2/s) respectively, as illustrated in Fig. 10(a). In the case of 150 °C aging, the values of k related to the IMC layers of SAC305/Cu-50Co and SAC305/Cu interface were 0.23654 and 0.18732 μm/h$^{1/2}$ (equal to $6.57 \times 10^{-17}$and 5.203×10^{-17} m^2/s), which were in accord with the previous results for Sn-3.5Ag-0.5Cu/Cu-8Zn solder joint, i.e. 5.42×10^{-17} m^2/s for aging at 150 °C [39]. Similarly, in the case of high temperature (180 °C) aging, the values of the diffusion coefficient k of these two interface were 0.68348 and 0.65389 μm/h$^{1/2}$ (equal to $1.9 \times 10^{-16}$and 1.816×10^{-16} m^2/s), respectively.

It can be clearly seen that the growth rate of IMCs of both SAC305/Cu-50Co and SAC305/Cu interfaces in Cu/SAC305/Cu-50Co solder joints was greatly affected by temperature during aging, and the higher temperature, the greater the growth rate of IMCs. While the difference of the diffusion coefficient of IMCs for SAC305/Cu and SAC305/Cu-50Co interfaces was increasingly reduced, as aging time and temperature increased. It was worth noting that the diffusion coefficient k of SAC305/Cu-50Co interface was slightly greater than that of SAC305/Cu interface. According to Figs. 4–6, the morphology of interfacial IMC layer on the side of Cu-50Co dual-phase substrate was uneven and irregular, as mentioned above, which was resulted from the reason that the reaction rate of Sn atoms with Cu atoms was faster than that of with Co atoms, and this difference became more and more evident as temperature increased during aging. Consequentially, at the SAC305/Cu-50Co interface, the rapid consumption of Cu-rich phase in Cu-50Co alloy substrate helped to expand the area of interfacial IMC layers, which in degree increased the thickness of IMC and exhibited a higher diffusion coefficient.

The growth activation energy of IMCs layer could be calculated by using the Arrhenius equation [40]:

$$D = D_0 \exp(-Q/RT) \quad (3)$$

Where D is the diffusion coefficient of IMC layer, D_0 is the IMC layer growth constant, Q is the activation energy for IMC during aging treatment, R is the universal gas constant (8.314 J/mol K), and T is the thermodynamic absolute temperature. According to the Arrhenius equation, Fig. 11 shows the Arrhenius plots for the IMC layers formed at the SAC305/Cu-50Co and SAC305/Cu interfaces, and the calculated interfacial IMC growth activation energies for SAC305/Cu-50Co and SAC305/Cu interfaces were 47.96 and 70.76 kJ/mol, respectively. The value of IMC activation energy at the SAC305/Cu interface was similar to that of 75.1 kJ/mol for IMC layers in SAC305/Cu joint aging at 100-170 °C [41]. It can be seen that activation energy of IMC layer at SAC305/Cu interface was higher than that of the IMC layer at SAC305/Cu-Co interface. The different initial IMC morphologies and thicknesses

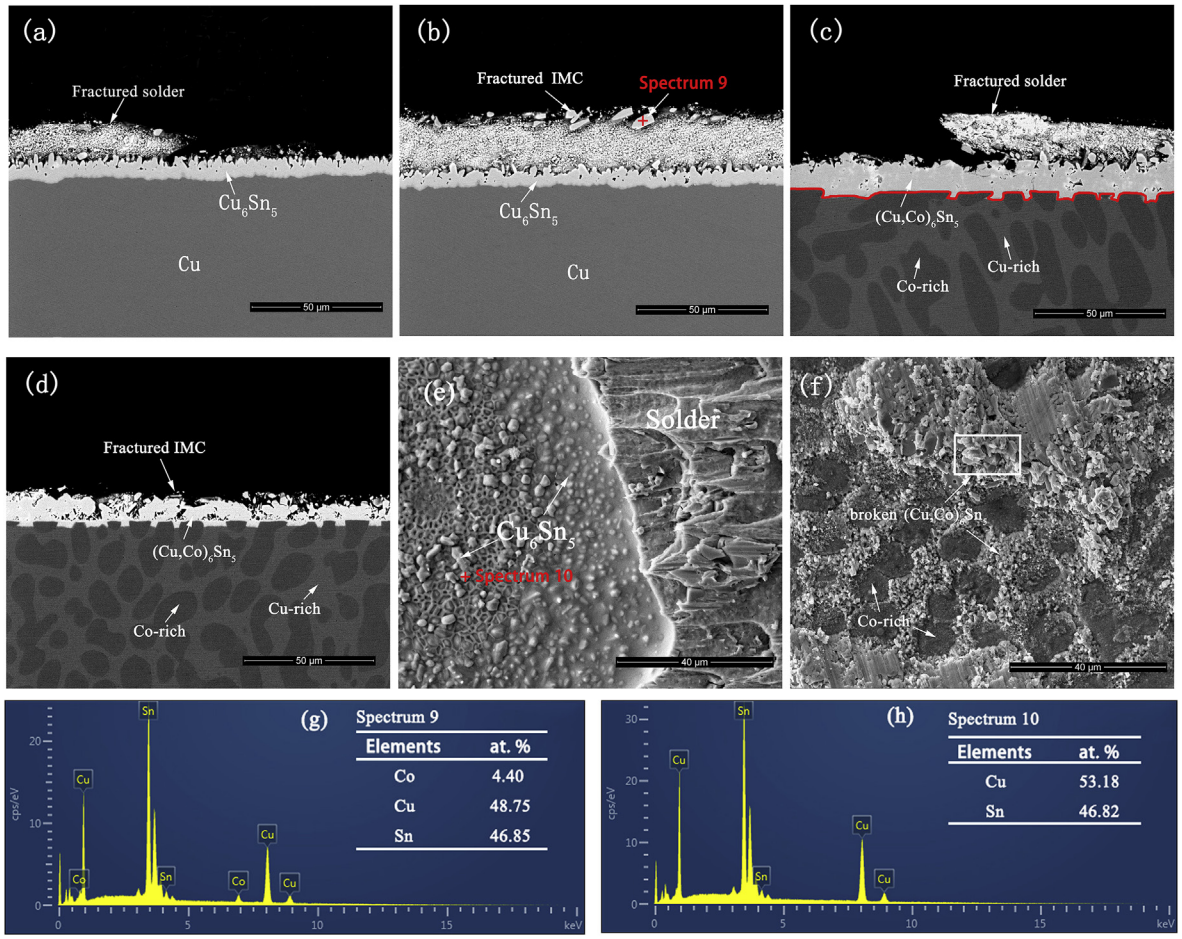

Fig. 14. The SEM photographs of Cu/SAC305/Cu-50Co solder joints after reflowing at 290 °C for 10 min subjected to shear fracturing, (a)-(b) the cross-sectional microstructure of SAC305/Cu interface, (c)-(d) the cross-sectional microstructure of SAC305/Cu-50Co interface, (e)-(f) the shear fracture top-view morphologies of the SAC305/Cu and SAC305/Cu-50Co interfaces, (g)-(h) the EDS results of spectrums 9 and 10.

would affect the results for the activity energies of IMC layer. Related references [42,43] pointed out that the lower activation energies on account of the higher layer-growth coefficients at low temperature are owing to the thinner initial layer. Therefore, in this study, although the initial thickness of IMC layer at SAC305/Cu-Co interface was thinner than that of IMC layer at SAC305/Cu interface after reflowing, the layer-growth coefficients of the former was greater than that of the latter.

3.3. Shear strength and fracture behavior

In order to preliminarily investigate the effect of interface morphology on the shear strength of the joints, a shear strength test was carried out between Cu/SAC305/Cu and Cu/SAC305/Cu-50Co solder joints by shear machine with the shear speed of 2000 μm/s. The shear test experiment is a universal method to analyze the reliability of a solder joint because the joints continually undergo mechanical loading during manufacturing and application [44]. The shear strengths of Cu/SAC305/Cu and Cu/SAC305/Cu-50Co solder joints after reflowing at 290 °C for 10 min were shown in Fig. 12.

In the case of reflowing at 290 °C for 10 min, the shear strength of Cu/SAC305/Cu solder joint was 49.2 MPa, while the shear strength of Cu/SAC305/Cu-50Co solder joint was 61.25 MPa. It might be concluded that the shear strength of Cu/SAC305/Cu-50Co solder joint was somewhat higher than that of Cu/SAC305/Cu solder joint. Fig. 13 illustrates the SEM photographs of the cross-section and top-view fracture morphologies of Cu/SAC305/Cu solder joints which were subjected to shear fracturing. As shown in Fig. 13(a), a layer of solder remained on the top of the Cu substrate, and a thin layer of IMC was observed on the top of solder nearby the fractured section. It can be seen that the failure of Cu/SAC305/Cu solder joint occurred mainly within the solder bulk and partly in the IMC layer. Fig. 13(b) indicated the magnified pictures of the regions marked with a red square in Fig. 13(a). It was apparently seen that the fractured Cu_6Sn_5 inside reaction IMC layer was above the solder at the SAC305/Cu interface, and the crack occurred within the Cu_6Sn_5 layer as marked by red circle in Fig. 13(b). Additionally, Fig. 13(c) and (d) show the top views of fracture surfaces of the samples and both of the IMC layer and solder appeared on the fracture surface. It can be seen that plenty of Cu_6Sn_5 grains were detected in IMC area, meanwhile numerous dimples were noticed in the solder bulk, which was similar to the results of previous literatures [45,46]. These dimples in fractured solder revealed that a great quantity of plastic deformation existed along the loading direction, which demonstrated that the obvious ductile fracture occurred within the solder bulk. Furthermore, there were some broken Cu_6Sn_5 grains could be detected at the bottom of dimples in solder bulk as presented in Fig. 13(d). The above observations obviously confirmed that the failure occurred mainly within solder bulk and partly in interfacial IMC layer, resulting in a mixed-mode fracture at the solder/Cu interface in the Cu/SAC305/Cu solder joints, which was also reported in previous study [47].

Fig. 14 shows the SEM micrographs of the cross-section and top-view fracture surfaces morphologies of failed Cu/SAC305/Cu-50Co solder joints. Fig. 14(a) and (b) show the cross-sectional microstructure

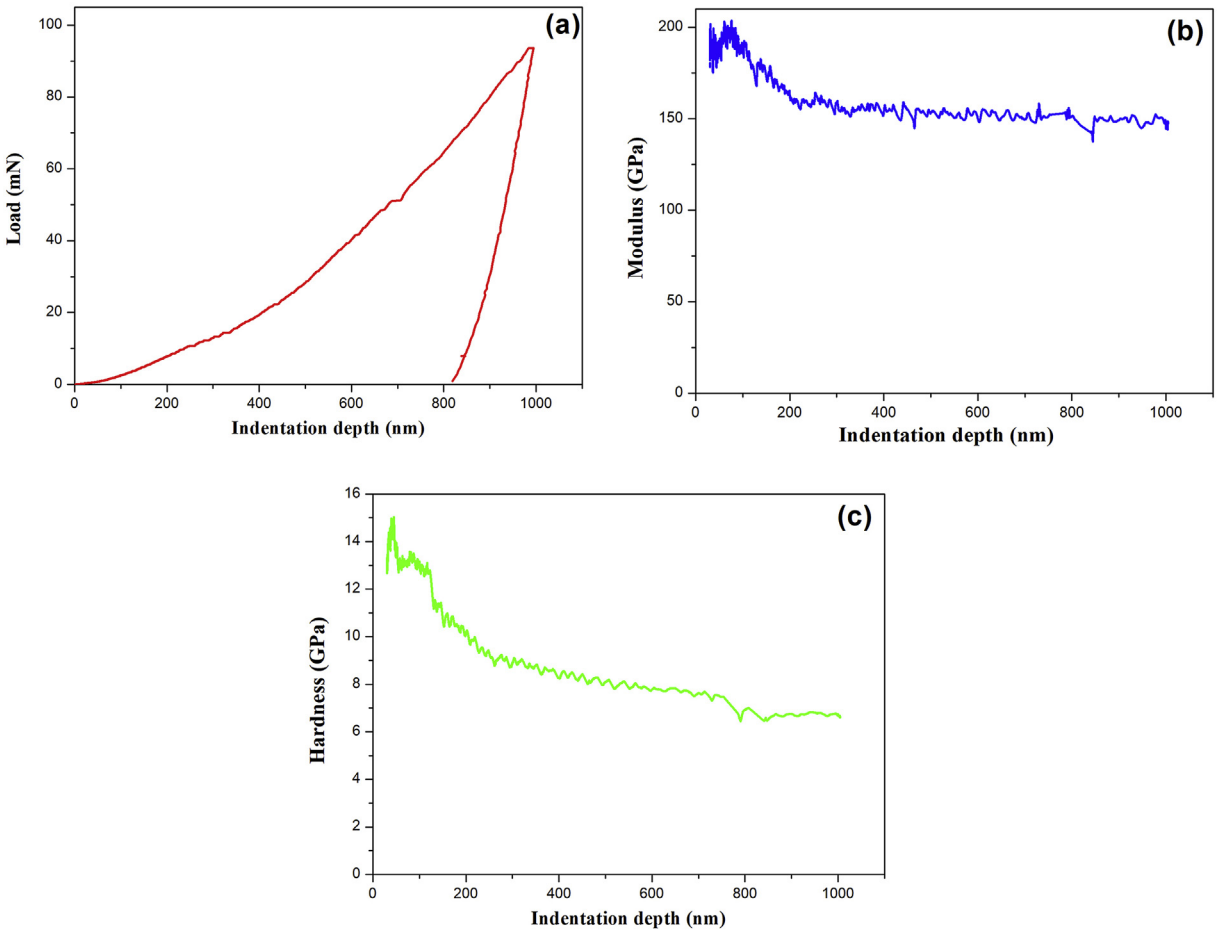

Fig. 15. (a) The load-depth curve of (Cu, Co)$_6$Sn$_5$ IMC, (b) The modulus-depth curve of (Cu, Co)$_6$Sn$_5$ IMC, (c) The hardness-depth curve of (Cu, Co)$_6$Sn$_5$ IMC.

Table 2
The modulus and hardness of Cu_6Sn_5 and (Cu, Co)$_6$Sn$_5$ IMCs obtained by nanoindentation.

IMC	Modulus (GPa)	Hardness (GPa)
Cu_6Sn_5	134 ± 7 [50]	6.5 ± 0.3 [50]
	116.89 ± 2.04 [51]	6.35 ± 0.20 [51]
(Cu, Co)$_6$Sn$_5$	151.62 ± 2.81	7.37 ± 0.33

of the pure Cu side of the fracture samples. According to these micrographs, it is observed that a portion of fractured residual solder covered the fracture surface and some Cu_6Sn_5 IMC was exposed on the fracture surface. It was noteworthy that a small amount fractured IMC was exposed above the solder due to shearing as shown in Fig. 14(b), and the composition of fractured IMC was determined by EDS analysis of Spectrum 9 in Fig. 14(g). It revealed that the IMC was composed of 48.75 at. % Cu, 46.85 at. % Sn and 4.4 at. % Co. As a result, the IMC phase was considered as (Cu, Co)$_6$Sn$_5$, which was the reaction product at the SAC305/Cu-50Co interface and partly remained in the fractured solder after shearing. Fig. 14(c)-(d) show the cross-sectional microstructure at the SAC305/Cu-50Co interface of the fractured solder joints. It can be seen that most of the (Cu, Co)$_6$Sn$_5$ IMC layers which were formed during reflowing, were exposed and fractured under the shear force. Besides, there was still a small amount of broken solder remaining in the upper IMC layer, and the amount of residual solder was less than that at the SAC305/Cu interface. Fig. 14(e) exhibits the shear fracture top-view morphology of the SAC305/Cu interface, and it was visually seen that there were two distinctly different types of fracture areas, which were identified as fractured IMC layer and solder, respectively. The surface of IMC layer area was covered by Cu_6Sn_5 IMC grains in Fig. 14(e), which were identified by the Spectrum 10 of EDS analysis as presented in Fig. 14(h). Additionally, some square lattice shapes appeared within the Cu_6Sn_5 grains in fractured IMC area, which might be caused by the fact that part of the Cu_6Sn_5 grains were taken away with the fracture of the bulk solder during the shear test. These observations further indicated that the fracture occurred at the SAC305/Cu interface following a mixed-mode fracture pattern. The shear fracture top-view morphology of the SAC305/Cu-50Co interface was shown in Fig. 14(f). It was clearly seen that most positions of fracture failure were inside the IMC layer and the (Cu, Co)$_6$Sn$_5$ IMC layers were entirely destroyed and exposed after shearing as indicated by the white square in Fig. 14(f). In addition to the observed broken (Cu, Co)$_6$Sn$_5$ grains, there were some Co-rich phase from the Cu-50Co alloy substrate appeared among the damaged (Cu, Co)$_6$Sn$_5$ grains, as shown by the dark parts in the Fig. 14(f). It is suggested that the formed (Cu, Co)$_6$Sn$_5$ IMC layer apparently dominated the failure fracture at the SAC305/Cu-50Co interface.

In order to further evaluate the mechanical properties of (Cu, Co)$_6$Sn$_5$ IMC, the nanoindentation of (Cu, Co)$_6$Sn$_5$ IMC was carried out. According to experimental results, load-depth, modulus-depth and hardness-depth curves had been fitted as illustrated in Fig. 15(a), (b) and (c), respectively, in which the indentations were perpendicular to the IMC layers. Particularly, Fig. 15(a) shows the load-depth curve of (Cu, Co)$_6$Sn$_5$ IMC with 0.2 s^{-1} strain rate at the maximum depth of 1000 nm. By averaging measurement data obtained over indentation depths ranging from 200 to 1000 nm, the values of modulus and hardness of (Cu, Co)$_6$Sn$_5$ obtained from indentations perpendicular to the IMC layers were found to be 151.62 ± 2.81 GPa and

7.37 ± 0.33 GPa, respectively, as listed in Table 2. It was noteworthy that the results of nanoindentation show that the values of modulus for (Cu, Co)$_6$Sn$_5$ (151.62 ± 2.81 GPa) was greater than that for Cu$_6$Sn$_5$ (133.7 GPa) according to previous research [48]. In addition, comparisons of (Cu, Co)$_6$Sn$_5$ results with Cu$_6$Sn$_5$ results reported by previous studies were exhibited in Table 2. It can be seen that both of modulus and hardness of (Cu, Co)$_6$Sn$_5$ were greater than those of Cu$_6$Sn$_5$. Moreover, Zhang et al. [49] pointed out that η'-Cu$_6$Sn$_5$ with Co substitutions should have a better ductility than the pure η'-Cu$_6$Sn$_5$ structure according to the results by using first-principles calculations. On the whole, the mechanical properties of (Cu, Co)$_6$Sn$_5$ were better than that of Cu$_6$Sn$_5$.

In summary, shear test results indicated that the shear strength of Cu/SAC305/Cu-50Co solder joint (61.25 MPa) was higher than that of Cu/SAC305/Cu solder joint (49.2 MPa). The uneven and jagged-shape IMC adjacent to the Cu-50Co dual-phase substrate (as indicated by red line in Fig. 14(c)) might contribute to the better adhesion strength between solder and substrate. The fracture surface of Cu/SAC305/Cu solder joints showed a mixed-mode fracture, and the failure occurred mainly within solder bulk and partly in Cu$_6$Sn$_5$ IMC layer at the SAC305/Cu interface. In the case of Cu/SAC305/Cu-50Co solder joint, the (Cu, Co)$_6$Sn$_5$ IMC layer mainly dominated the failure fracture, numerous broken (Cu, Co)$_6$Sn$_5$ grains and some Co-rich phase were observed at the SAC305/Cu-50Co fracture surface. In addition, part of the fracture occurred within solder bulk, the addition of Co atoms promoted the formation of small amounts of (Cu, Co)$_6$Sn$_5$ in solder, which also increased the mechanical properties of the solder and the shear strength of joint. The nanoindentation results show that both of modulus and hardness of (Cu, Co)$_6$Sn$_5$ were greater than those of Cu$_6$Sn$_5$. In this case, it primarily proved that the strength of Cu$_6$Sn$_5$ IMC formed at SAC305/Cu interface in Cu/SAC305/Cu solder joints was weaker than that of (Cu, Co)$_6$Sn$_5$ IMC formed at the SAC305/Cu-50Co interface in Cu/SAC305/Cu-50Co solder joints.

4. Conclusions

In this study, we investigated the interfacial reaction of interfacial IMCs layer in Cu/SAC305/Cu-50Co solder joints during reflowing at 290 °C and solid-state aging at different temperatures for various time. Additionally, the shear experiments for Cu/SAC305/Cu and Cu/SAC305/Cu-50Co solder joints were carried out. The following conclusions can be drawn from the present research:

(1) For Cu/SAC305/Cu-50Co solder joints, after reflowing, the elongated shape (Cu, Co)$_6$Sn$_5$ IMC layer was observed at the SAC305/Cu-50Co interface. The (Cu, Co)$_6$Sn$_5$ IMC layer adjacent to the Cu-50Co alloy substrate showed an uneven and serrated-shape, while a single scallop-shaped Cu$_6$Sn$_5$ IMC layer could be found at the SAC305/Cu interface.
(2) During solid-state aging, the thickness of IMCs at both of two interfaces continually increased, and the difference of the diffusion coefficient of both interfaces was increasingly reduced as aging time and temperature increased. The (Cu, Co)$_3$Sn phase was formed between (Cu, Co)$_6$Sn$_5$ IMC and Cu-50Co substrate, while Cu$_3$Sn IMC was observed at the interface between Cu$_6$Sn$_5$ layer and Cu substrate. The Kirkendall voids were observed clearly at the SAC305/Cu-50Co interface. The activation energies of the total IMC at SAC305/Cu and SAC305/Cu-50Co interfaces were 70.76 and 47.96 kJ/mol, respectively.
(3) The shear strength of Cu/SAC305/Cu solder joint (49.2 MPa) was slightly lower than that of the Cu/SAC305/Cu-50Co solder joint (61.25 MPa) after reflowing process. The fracture surface of Cu/SAC305/Cu solder joints showed a mixed-mode fracture, while the (Cu, Co)$_6$Sn$_5$ IMC layer mainly dominated the failure fracture at the SAC305/Cu-50Co interface in Cu/SAC305/Cu-50Co solder joints.

Acknowledgements

This work was supported by the National Natural Science Foundation of China (No. 51765040), Natural Science Foundation of Jiangxi Province (20161BAB206122 and 20161BAB206128).

References

[1] Guang Chen, Fengshun Wu, Changqing Liu, Weisheng Xia, Hui Liu, Effects of fullerenes reinforcement on the performance of 96.5Sn-3Ag-0.5Cu lead-free solder, Mater. Sci. Eng. A 636 (2015) 484–492.
[2] Nianduan Lu, Donghua Yang, Liangliang Li, Interfacial reaction between Sn-Ag-Cu solder and Co-P films with various microstructures, Acta Mater. 61 (2013) 4851-4590.
[3] Y. Fujiwara, H. Enomoto, T. Nagao, H. Hoshika, Composite plating of Sn-Ag alloys for Pb-free soldering, Surf. Coating. Technol. 169–170 (2003) 100–103.
[4] Chaohong Wang, Chunchieh Wen, Cheyang Lin, Solid-state interfacial reactions of Sn and Sn-Ag-Cu solders with an electroless Co(P) layer deposited on a Cu substrate, J. Alloy. Comp. 662 (2016) 475–483.
[5] Chao Li, Xiaowu Hu, Xiongxin Jiang, Yulong Li, Interfacial reaction and microstructure between the Sn3Ag0.5Cu solder and Cu-Co dual-phase substrate, Appl. Phys. A 124 (2018) 484.
[6] Donghua Yang, Guoshuai Yang, Jian Cai, Qian Wang, Jingwei Li, Yang Hu, Liangliang Li, Kinetics of interfacial reaction between Sn-3.0Ag-0.5Cu solder and Co-4.0P or Co-8.0P metallization, International Conference on Electronic Packaging Technology,2015 16th.
[7] Xiaowu Hu, Tao Xu, Leon M. Keer, Yulong Li, Xiongxin Jiang, Microstructure evolution and shear fracture behavior of aged Sn3Ag0.5Cu/Cu solder joints, Mater. Sci. Eng. A 673 (2016) 167–177.
[8] T. Laurila, V. Vuorinen, J.K. Kivilahti, Interfacial reactions between lead-free solders and common base materials, Mater. Sci. Eng. R. 49 (2005) 1–60.
[9] Xiaowu Hu, Yulong Li, Yong Liu, Yi Liu, Zhixian Min, Microstructure and shear strength of Sn37Pb/Cu solder joints subjected to isothermal aging, Microelectron. Reliab. 54 (2014) 1575–1582.
[10] K. Suganuma, Advances in lead-free electronics soldering, Curr. Opin. Solid State Mater. Sci. 5 (2001) 55–64.
[11] Wen-Hwa Chen, Ching-Feng Yu, Hsien-Chie Cheng, Yu-min Tsai, Su-Tsai Lu, IMC growth reaction and its effects on solder joint thermal cycling reliability of 3D chip stacking packaging, Microelectron. Reliab. 53 (2013) 30–40.
[12] Y.J. Chen, C.K. Chung, C.R. Yang, C.R. Kao, Single-joint shear strength of micro Cu pillar solder bumps with different amounts of intermetallics, Microelectron. Reliab. 53 (2013) 47–52.
[13] T.H. Chuang, C.C. Jain, H.M. Wu, Intermetallic reactions in Sn-0.4Co-0.7Cu solder BGA packages with an ENIG surface finish, J. Electron. Mater. 37 (2008) 1734–1741.
[14] An Tong, Fei Qin, Effects of the intermetallic compound microstructure on the tensile behavior of Sn3.0Ag0.5Cu/Cu solder joint under various strain rates, Microelectron. Reliab. 54 (2014) 932–938.
[15] C. Andersson, P. Sun, J. Liu, Tensile properties and microstructural characterization of Sn-0.7Cu-0.4Co bulk solder alloy for electronics applications, J. Alloy. Comp. 457 (2008) 97–105.
[16] Chi Yang Yu, Kai Jheng Wang, Jenq Gong Duh, Interfacial reaction of Sn and Cu-xZn substrates after reflow and thermal aging, J. Electron. Mater. 39 (2010) 230–237.
[17] Moon Gi Cho, Sun-Kyoung Seo, Hyuck Mo Lee, Wettability and interfacial reactions of Sn-based Pb-free solders with Cu-xZn alloy under bump metallurgies, 474 (2009) 510–516.
[18] Fengjiang Wang, Dongyang Li, Jiheng Wang, Xiaojing Wang, Comparative study on the wettability and interfacial structure in Sn-xZn/Cu and Sn/Cu-xZn system, J. Mater. Sci. Mater. Electron. 28 (2017) 1631–1643.
[19] Chao-hong Wang, ChunyiKuo, Interfacial reactions between eutectic Sn-Pb solder and Co substrate, J. Mater. Sci. 46 (2011) 2654–2661.
[20] Chao-hong Wang, ChunyiKuo, Growth kinetics of the solid-state interfacial reactions in the Sn-Cu/Co and Sn/Co-Cu couples, Mater. Chem. Phys. 130 (2011) 651–656.
[21] Chaohong Wang, Chunyi Kuo, Shengen Huang, Poyi Li, Temperature effects on liquid-state, Sn/Co Interfacial React. 32 (2013) 57–63.
[22] W. Yang, Z.F. Xu, W.J. Li, C.C. Cai, S. Li, F. Liu, G.C. Yang, Comparisons of grain refinement and recalescence behavior during the rapid solidification of undercooled Cu-Co and Cu-Ni alloys, Physica B 406 (2011) 3710–3714.
[23] Wei Yang, Yan Long Zhang, He Wen, Zhi Feng Xu, Effects of copper content and liquid separation on the microstructure formation of Co-Cu alloys, Int. J. Mater. Res. 105 (2014) 861–868.
[24] W. Yang, S.H. Chen, H. Yu, S. Li, F. Liu, G.C. Yang, Effects of liquid separation on the microstructure formation and hardness behavior of undercooled Cu-Co alloy, Appl. Phys. A 109 (2012) 665–671.
[25] W. Yang, H. Yu, J.H. Wang, C.C. Cai, Z.F. Xu, S. Li, F. Liu, G.C. Yang, Application of dendrite fragmentation to fabricate the homogeneous dispersed structure in undercooled Cu-Co immiscible alloy, J. Alloy. Comp. 509 (2011) 9675–9678.
[26] S.J. Wang, C.Y. Liu, Study of interaction between Cu-Sn and Ni-Sn interfacial reactions by Ni-Sn3.5Ag-Cu sandwich structure, J. Electron. Mater. 32 (2003) 1303–1309.
[27] Guang Zeng, Stuart D. McDonald, Qinfen Gu, Yasuko Terada, Kentaro Uesugi,

Hideyuki Yasuda, Kazuhiro Nogita, The influence of Ni and Zn additions on microstructure and phase transformations in Sn-0.7Cu/Cu solder joints, Acta Mater. 83 (2015) 357–371.
[28] Guang Zeng, Stuart D. McDonald, Dekui Mu, Yasuko Terada, Hideyuki Yasuda, Qinfen Gu, Kazuhiro Nogita, Ni segregation in the interfacial (Cu, Ni)$_6$Sn$_5$ intermetallic layer of Sn-0.7Cu-0.05Ni/Cu ball grid array (BGA) joints, Intermetallics 54 (2014) 20–27.
[29] H.J. Dong, Z.L. Li, X.G. Song, H.Y. Zhao, J.C. Yan, H. Tian, J.H. Liu, Grain morphology and mechanical strength of high-melting-temperature intermetallic joints formed in asymmetrical Ni/Sn/Cu system using transient liquid phase soldering process, J. Alloy. Comp. 723 (2017) 1026–1031.
[30] Yueting Chen, Yating Chan, Chihchi Chen, Wettability and interfacial reactions between the molten Sn-3.0wt%Ag-0.5wt%Cu solder (SAC305) and Ni-Co alloys, J. Alloy. Comp. 507 (2010) 419–424.
[31] Hao Chen, Yi-Ling Tsai, Yu-Ting Chang, Albert T. Wu, Effect of massive spalling on mechanical strength of solder joints in Pb-free solder reflowed on Co-based surface finishes, J. Alloy. Comp. 671 (2016) 100–108.
[32] J.H. Hong, H.Y. Lee, Albert T. Wu, Massive spalling and morphological change of intermetallic compound affected by adding Pd in Co-based surface finishes, J. Alloy. Comp. 580 (2013) 195–200.
[33] Phase Diagram, second ed., ASM International, Materials Park, OH, 1990.
[34] Hailong Li, An Rong, Chunqing Wang, Yanhong Tian, Zhi Jiang, Effect of Cu grain size on the voiding propensityat the interface of SnAgCu/Cu solder joints, Mater. Lett. 144 (2015) 97–99.
[35] Dezhi Li, Changqing Liu, Paul P. Conway, Characteristics of intermetallics and micromechanical properties during thermal ageing of Sn-Ag-Cu flip-chip solder interconnects, Mater. Sci. Eng. A 391 (2005) 95–103.
[36] M. Ousama, Abdelhadi, Leila Ladani, IMC growth of Sn-3.5Ag/Cu system: combined chemical reaction and diffusion mechanisms, J. Alloy. Comp. 537 (2012) 87–99.
[37] Shuai Li, Yanfu Yan, Intermetallic growth study at Sn-3.0Ag-0.5Cu/Cu solder joint interface during different thermal conditions, J. Mater. Sci. Mater. Electron. 26 (2015) 9470–9477.
[38] Tao Xu, Xiaowu Hu, Yulong Li, Xiongxin Jiang, The growth behavior of interfacial intermetallic compound between Sn-3.5Ag-0.5Cu solder and Cu substrate under different thermal-aged conditions, J. Mater. Sci. Mater. Electron. 28 (2017) 18515–18528.
[39] Yu Xiao, Xiaowu Hu, Yulong Li, Ruhua Zhang, Effect of alloying Cu substrate on microstructure and coarsening behavior of Cu_6Sn_5 grains of soldered joints, J. Mater. Sci. Mater. Electron. 26 (2015) 2782–2794.
[40] John H.L. Pang, Luhua Xu, X.Q. Shi, W. Zhou, S.L. Ngoh, Intermetallic growth studies on Sn-Ag-Cu lead-free solder joints, J. Electron. Mater. 33 (2004) 1219–1226.
[41] Jeong-Won Yoon, Bo-In Noh, Bong-kyun Kim, Chang-Chae Shur, Seung-Boo Jung, Wettability and interfacial reactions of Sn-Ag-Cu/Cu and Sn-Ag-Ni/Cu solder joints, J. Alloy. Comp. 486 (2009) 142–147.
[42] Liang Zhang, Xi-ying Fan, He Cheng-wen, Yong-huan Guo, Intermetallic compound layer growth between SnAgCu solder and Cu substrate in electronic packaging, J. Mater. Sci. Mater. Electron. 24 (2013) 3249–3254.
[43] D.Q. Yu, C.M.L. Wu, C.M.T. Law, L. Wang b, J.K.L. Lai, Intermetallic compounds growth between Sn-3.5Ag lead-free solder and Cu substrate by dipping method, J. Alloy. Comp. 392 (2005) 192–199.
[44] Xiaowu Hu, Tao Xu, Leon M. Keer, Yulong Li, Xiongxin Jiang, Shear strength and fracture behavior of reflowed Sn3.0Ag0.5Cu/Cu solder joints under various strain rates, J. Alloy. Comp. 690 (2017) 720–729.
[45] Hwa-Teng Lee, Ming-Hung Chen, Huei-Mei Jao, Tain-Long Liao, Influence of interfacial intermetallic compound on fracture behavior of solder joints, Mater. Sci. Eng. A 358 (2003) 134–141.
[46] Dae-Gon Kim, Jong-Woong Kim, Seung-Boo Jung, Effect of aging conditions on interfacial reaction and mechanical joint strength between Sn-3.0Ag-0.5Cu solder and Ni-P UBM, Mater. Sci. Eng. B 121 (2005) 204–210.
[47] Xiaowu Hu, Wenjing Chen, Yu Xiao, Yulong Li, Yi Liu, Zhixian Min, Shear strengths and fracture behaviors of Cu/Sn37Pb/Cu soldered joints subjected to different displacement rates, J. Alloy. Comp. 600 (2014) 13–20.
[48] C. Sous, G. Jacobs, T. Lutz, Characterisation of elastic-plastic material characteristics of Sn solid solution, SbSn and Cu_6Sn_5 in the tin-based sliding bearing alloy SnSb12Cu6ZnAg, Mater. Sci. Eng. A 724 (2018) 566–575.
[49] Xuechao Zhang, Xiuchen Zhao, Bing Zheng, Ying Liu, Jingwei Cheng, Li Hong, First-principles study of thermodynamical and elastic properties of η'-$(Cu,Co)_6Sn_5$ ternary alloys, J. Electron. Mater. 45 (2016) 4919–4927.
[50] Pingfeng Yang, Yishao Lai, Shengrui Jian, Jiunn Chen, Rongsheng Chen, Nanoindentation identifications of mechanical properties of Cu_6Sn_5, Cu_3Sn, and Ni_3Sn_4 intermetallic compounds derived by diffusion couples, Mater. Sci. Eng. A 485 (2008) 305–310.
[51] R.R. Chromik, R.P. Vinci, S.L. Allen, M.R. Notis, Nanoindentation measurements on Cu-Sn and Ag-Sn intermetallics formed in Pb-free solder joints, J. Mater. Res. 18 (2003) 2251–2261.